Articles

Kinetics and Consequences of Binding of Nona- and Dodecapeptides to the Oligopeptide Binding Protein (OppA) of *Lactococcus lactis*†

Frank C. Lanfermeijer,‡ Antonia Picon, Wil N. Konings, and Bert Poolman*,§

Groningen Biomolecular Sciences and Biotechnology Institute, University of Groningen, Kerklaan 30, NL-9751 NN, Haren, The Netherlands

Received June 28, 1999; Revised Manuscript Received September 2, 1999

ABSTRACT: The oligopeptide transport system (Opp) of *Lactococcus lactis* belongs to the class of binding protein-dependent ABC-transporters. This system has the unique capacity to mediate the uptake of peptides from 4 up to at least 18 residues. Kinetic analysis of peptide binding to the binding protein, OppA*, revealed a relationship between the peptide dissociation constants and the length of the ligand. The dissociation constants varied from submicromolar for dodecapeptides to millimolar for pentapeptides. This implies that the residues 6−12 of the peptide contribute to the binding affinity, and, in contrast to the current views on peptide binding by homologous proteins, these residues must interact with OppA*. Analysis of pre-steady-state kinetics of binding showed that the observed differences in the K_d^L-values result primarily from variations in the dissociation rate constants. These results are discussed in relation to the affinity constant for transport of these substrates. Overall, the data suggest that the slow dissociation rate constants for the larger peptides are rate determining in the translocation of peptides across the membrane.

The superfamily of ABC[1] transporters mediates transport of solutes as diverse as lipophilic cytotoxins, inorganic ions, carbohydrates, peptides, and others (*1*). A distinct class within the ABC superfamily is formed by the binding protein-dependent transport systems (*2*, *3*). Uptake by these systems depends on the presence of a ligand-binding protein at the outer surface of the cytoplasmic membrane, which provides specificity and, usually, a high affinity to the transport process. The binding proteins of peptide transport systems consist of two major domains and one minor domain (*4*, *5*). The binding site of these proteins is formed by a cleft between the two major domains, which are connected by a flexible hinge. Upon ligand binding, the protein undergoes a major conformational change, which results in closure of the cleft and occlusion of the ligand. This binding mechanism is referred to as the "Venus's-flytrap" mechanism (*6*, *7*). The third domain is unique for the peptide binding proteins, but to date no function has been ascribed to this domain.

The best-studied peptide binding proteins are those of the dipeptide transporter (Dpp) of *Escherichia coli* (*4*, *8*) and the oligopeptide transporter (Opp) of *Salmonella typhimurium* (*5*, *9*−*11*). From the structural analysis of these binding proteins (DppA and OppA), it is apparent that the prerequisites for ligand binding are an unmodified peptide backbone and a free amino- and carboxyl-terminus of the peptide. The side chains are accommodated in a maximum of five binding pockets that each has the capacity to harbor every type of amino acid side chain. Although some specificity studies have been performed, the pre-steady-state kinetics of ligand binding has not been studied for any peptide-binding protein.

ABC-type (oligo)peptide transport systems are present in most if not all bacteria. The so far unique feature of the oligopeptide transport system (Opp) of *Lactococcus lactis* relates to its capacity to mediate the uptake of oligopeptides from 4 to at least 18 amino acid residues (*12*). In situ, the substrates for the transport system result from the hydrolysis of exogenous proteins (*13*). As these peptide fragments range in size from 4 to 30 amino acid residues, the Opp-system of *L. lactis* may have evolved to allow the utilization of these extremely long peptides.

In this paper, we report on the interaction of peptides, ranging in size from 5 to 12 amino acid residues, that were previously shown to be transported by Opp of *L. lactis* (*12*, *13*), with the binding protein of the system. The specificity of peptide binding was assessed by using native cationic gel electrophoresis and intrinsic protein fluorescence, and they

† This work is supported by grants from the European Union (Bio-4-CT-960016 and FAIR-CT-965030) and the Gratama Foundation (NL).

* To whom correspondence should be addressed. Phone: +31 50 3632170. Fax: +31 50 3632154. E-mail: B.Poolman@chem.rug.nl.

‡ Present address: Department of Molecular Biology of Plants; Groningen Biomolecular Sciences and Biotechnology Institute; University of Groningen; Kerklaan 30; NL-9751 NN, Haren; The Netherlands.

§ Present address: Department of Biochemistry, Groningen Biomolecular Sciences and Biotechnology Institute, University of Groningen, Nijenborgh 4, NL-9747 AG Groningen, The Netherlands. Email: b.poolman@chem.rug.nl.

[1] Abbreviations: ABC, ATP-binding cassette; OD_{660}, optical density at 660 nm.

10.1021/bi9914715 CCC: $18.00
Published on Web 10/16/1999

include the first pre-steady-state kinetic analysis of ligand binding to this type of protein. The data obtained are discussed in relation to the observed uptake kinetics as described by Detmers et al. (*12*).

EXPERIMENTAL PROCEDURES

Bacterial Strains and Plasmids. The plasmid pAMP21 was derived from pGKOppAChis by replacing the *lacS*-promoter of *Streptococcus thermophilis* by the lactococcal p32-promoter (Picon, A., Lanfermeijer, F. C., Kunji, E. R. S., Konings, W. N., and Poolman, B., unpublished results). The coding sequence of OppA* was placed in frame with a carboxyl-terminal factor Xa cleavage site and a 6-histidine tag. Plasmid pAMP21 was transformed into *L. lactis* AMP2 using electrotransformation. Strain AMP2 (Picon, A., Lanfermeijer, F. C., Kunji, E. R. S., Konings, W. N., and Poolman, B., unpublished results) is isogenic to strain IM15 (*14*), except that the *oppA*-gene has been deleted from the chromosome.

Cell Growth. L. lactis strain AMP2/pAMP21 was grown in 1/2×M17 Broth (Difco), pH 6.0, supplemented with 0.5% glucose plus 5 μg/mL erythromycin in a 10 L ADI 1065 fermentor (Applikon Dependable Instruments, B. V. Schiedam) with pH control. Cells were harvested in the late exponential phase of growth, washed twice with 25 mM potassium phosphate, pH 6.0, and resuspended to an OD_{660} of ~500 in the same buffer. Cells were frozen in liquid nitrogen and stored at −80 °C.

*Purification of OppA**. Frozen cells were thawed at room temperature and incubated at 30 °C for 30 min, which facilitated the breakage of the cells, possibly as a result of activation of lytic activity in the cell wall. Next, the cell suspension was diluted 5-fold with 25 mM potassium phosphate, pH 6.0, and KCl was added to a final concentration of 100 mM. The cells were broken by three consecutive French press steps at 20 000 psi at 4 °C. After the first and third step, phenylmethanesulfonyl fluoride in 2-propanol was added to a final concentration of 0.1 mM. Subsequently, $MgSO_4$ was added to 10 mM, and the solution was incubated with 100 μg/mL deoxyribonuclease type I at 37 °C for 15 min. Unbroken cells and cell debris were removed by centrifugation for 15 min at 11000*g*. The cell-free homogenate was centrifuged for 15 min at 290000*g*, and the supernatant was collected. The supernatant still contained nucleic acids, as was assessed by spectrophotometry. These polymers interfere with the purification procedure, and therefore, the following anion-exchange step was included in the procedure. A 10 mL Source 30Q column (Pharmacia) was equilibrated with 200 mM KCl in buffer A (25 mM potassium phosphate, pH 6.0, with 10% v/v glycerol) and the supernatant was loaded. The column was washed with 200 mM KCl in buffer A until the absorbance at 280 nm returned to the baseline value, where after the column was washed with 400 mM KCl in buffer A. The flow-through and the 200 mM KCl eluate were pooled (low-salt fraction). As judged by Western blot analysis (data not shown), both the low-salt fraction (approximately 70% of the final yield) and the 400 mM KCl eluate (high salt fraction) contained OppA*. Both fractions were diluted with buffer A to a final KCl concentration of 100 mM and loaded separately onto a 1 mL Resource S column (Pharmacia), which was equilibrated with 100 mM KCl in buffer A. In both cases, OppA* eluted from the column at 270 mM KCl when a gradient of KCl in buffer A was applied.

Removal of Endogenous Ligand. Co-purified ligand, bound to OppA*, was removed by immobilizing the protein to a nickel-nitrilotriacetic acid (Ni^{2+}-NTA) agarose column. The Ni^{2+}-NTA agarose was equilibrated with 270 mM KCl in buffer A, and the pooled fractions of the Resource S column were loaded onto the Ni^{2+}-NTA resin. Four column volumes of buffer A, pH 7.5, plus 100 mM KCl were passed over the column, and, subsequently, the column was washed with 40 column volumes of buffer A, pH 7.5, supplemented with 2 M guanidinium-HCl (Gdm). Next, the Gdm was removed by decreasing the Gdm in the washing buffer in three steps of 4 column volumes (1.5, 1.0, and 0.5 M, final concentration of Gdm), followed by 8 column volumes of buffer A plus 100 mM KCl, pH 7.5. Finally, OppA* was eluted from the resin using buffer A, pH 6.0, plus 100 mM KCl and 300 mM histidine-HCl. Approximately 70−80% of the loaded protein was recovered. Histidine was removed in a Bio-Rad PD10 desalting step, and when necessary, the protein was concentrated in an Amicon Centricon concentrator with a molecular mass cutoff of 30 kDa. The protein was stable for at least 3 months at 4 °C and at least for several days at room temperature in MP-buffer (buffer A, pH 6.0, supplemented with 1 mM K-EDTA and 100 mM KCl).

SDS−PAGE and Immunodetection. Electrophoresis was performed according to the method of Laemmli (*15*) on a Mini-Protean II system (Bio-Rad). The discontinuous gel system consisted of a 6% stacking gel and a 10% resolving gel. Cross-linkage was 2.6% in both gels. After electrophoresis gels were stained with Coomassie Brilliant Blue.

Native Cationic Gel Electrophoresis. Native cationic electrophoresis (NCE) was performed according to a modification of the method of Reisfield et al. (*16*). Briefly, the discontinuous gel system consisted of a 4% stacking gel and a 10% resolving gel in 0.06 M KOH-acetate buffers at pH 6.5 and 4.5, respectively. Polymerization was performed with ammoniumpersulfate and *N*,*N*,*N*′,*N*′-tetramethyl-ethylenediamine, and the percentage cross-linking was 2.6% in both gels. The electrode buffer was composed of 0.35 M β-alanine, adjusted to pH 4.5 with acetic acid. Protein samples (1 μg) in 10 μL of MP-buffer were loaded, after the addition of a small grain of Methyl Green tracking dye. Proteins were separated by electrophoresis from the anode to the cathode at a constant voltage of 100 mV.

Steady-State Fluorescence. Fluorescence spectra were obtained with an Aminco 4800 spectrofluorimeter. A quartz-cuvette contained 1 mL of an OppA* solution (0.5−2 μM) in filtered and thoroughly degassed MP-buffer, which was continuously stirred and kept at 15 °C with a circulating waterbath. Emission spectra were obtained by excitation at 280 nm with slit widths of 2 nm. Effects of peptides on fluorescence were measured by exciting at 280 nm with a slit width of 2 nm and measuring the emission at 315 nm with a slit width of 8 nm.

The binding curves were analyzed in three ways. First, when the K_d^L-values were at least five times larger than the protein concentration, the changes in fluorescence (ΔF) as a function of peptide concentration were analyzed according to a hyperbolic binding equation:

$$\Delta F = \frac{\Delta F_{max} L}{K_d^L + L} \quad (1)$$

where ΔF is the observed fluorescence at the peptide concentration L, L is the total peptide concentration, ΔF_{max} is the fluorescence change at infinite peptide concentration, and K_d^L is the equilibrium dissociation constant. Second, when the K_d^L-values appeared to be smaller than the OppA* concentration, the binding curves were analyzed by the general equilibrium binding equation (*17*) for a binding stoichiometry of 1:

$$\Delta F = \Delta F_{max} \frac{(1 + K_d^L/P_0 + L/P_0) - \sqrt{(1 + K_d^L/P_0 + L/P_0)^2 - 4L/P_0}}{2} \quad (2)$$

where L, ΔF, ΔF_{max}, and K_d^L have the same meaning as above and where P_o is the total protein concentration. Third, when K_d^L-values and the OppA concentration were in the same range, both procedures were applied, with the exception that in the case of analyzing the data by the hyperbolic binding equation, the free peptide concentration was used, and a reiterative fit procedure was applied. Both procedures gave very similar values, also when peptide binding was analyzed at different protein concentrations (around and above the K_d). Nonlinear least-squares regression was performed with the program of SigmaPlot (Jandel Scientific Software).

Rapid-Binding Kinetics. Rapid kinetic experiments were performed with an SX-17 MV Stopped-Flow spectrofluorimeter from Applied Photophysics. The reaction cell path was 1.2 cm, which resulted in a deadtime of approximately 1.7 ms. The volume of the reaction chamber was 150 μL. Temperature was set at 15 °C. The excitation wavelength was 280 nm and emission was detected with a photomultiplier tube. A 305 nm cutoff filter was placed between the reaction cell and the photomultiplier tube. The association process was initiated by rapidly mixing equal volumes of an OppA-solution (1 μM) and a peptide solution of the desired concentration in MP-buffer. The dissociation process was initiated by rapidly mixing 1 vol of a 3 μM OppA*-solution in MP-buffer, supplemented with the desired peptide, and 5 vol of MP-buffer. In one experiment, three to five separate traces for each peptide concentration were averaged and subsequently analyzed. In case of the peptides SLSQSKVLP and RDMPIQAF, the association process was analyzed according to the following equation:

$$\Delta F_t = \Delta F_{eq}(1 - e^{-k_{obs}t}) \quad (3)$$

where ΔF_t is the fluorescence change at a given time, ΔF_{eq} is the fluorescence change at equilibrium, and k_{obs} is the observed rate constant of the process, which is a function of the association (k_{+1}) and dissociation (k_{-1}) rate constants according to

$$k_{obs} = Lk_{+1} + k_{-1} \quad (4)$$

where L is the concentration of the ligand. In case of the peptide SLSQSKVLPVPQ, the association process was analyzed with the following equation:

$$\Delta F_t = \Delta F_1(1 - e^{-k_{obs1}t}) - \Delta F_2(1 - e^{-k_{obs2}t}) \quad (5)$$

where ΔF_t is the fluorescence change at a given time, and ΔF_1 and ΔF_2 reflect the fluorescence change associated with the fast and slow process, respectively. The constants k_{obs1} and k_{obs2} are the observed rate constants of the fast and slow process, respectively.

The dissociation process of the peptides SLSQSKVLP and RDMPIQAF was analyzed according to

$$\Delta F_t = \Delta F_{eq} e^{-k_{obs}t} \quad (6)$$

where ΔF_t is the fluorescence change at a given time, ΔF_{eq} is the fluorescence change at equilibrium, and k_{obs} is the observed rate constant of the process, which is also a function of k_{-1} and k_{+1} (eq 4). Analysis was performed using the supplied Biosequential SX-18 MV, version 4.22 Stopped-Flow reaction Analyzer analysis software from Applied Photophysics.

Kinetic Analysis. A relationship between K_d^L of the binding protein for its ligand and the K_m for the binding protein dependent transport reaction is derived in this section; the general description is given in the Discussion. The rate of transport, under the conditions that the donation step is rate determining (step III in Figure 1), is given by

$$v = k'_{+2} \cdot EL{:}M \quad (7)$$

In this case, the transport intermediates left of the donation step will equilibrate according to their equilibrium constants:

$$K_d^L = \frac{E \cdot L}{EL} \Rightarrow EL = \frac{E \cdot L}{K_d^L} \quad (8)$$

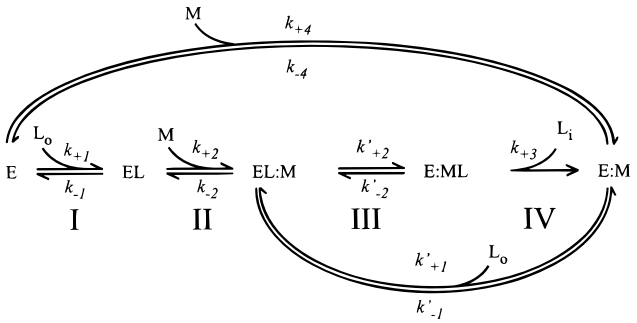

FIGURE 1: Kinetic model for the transport of a peptide via a binding protein dependent transport system. Where E and EL represent the unloaded and liganded binding protein, respectively, L_o and L_i are the external and internalized substrate, respectively, and M refers to the membrane complex. The species EL:M and E:M represent loaded and unloaded binding proteins docked to membrane complex, respectively. E:ML refers to the situation in which the ligand is transferred to the membrane complex and the binding protein is still docked. In Detmers et al. (*12*), E_1L and E_2L correspond to EL and EL:M. The following steps are discriminated in the model: I, binding of ligand to the binding protein; II, docking of the liganded binding protein to the membrane complex; III, donation of the ligand to the membrane complex; IV, translocation of substrate across the membrane. The branch with the constants k'_{+1} and k'_{-1} provides an explanation for the sigmoidial uptake kinetics (see ref *12*).

$$K_d^{EL} = \frac{EL \cdot M}{EL:M} \Rightarrow M = \frac{K_d^{EL} \cdot EL:M}{EL} \quad (9)$$

K_d^L represents the equilibrium constant for binding of the ligand to the binding protein (equals k_{-1}/k_{+1} in Figure 1), and K_d^{EL} represents the equilibrium constant for binding of the liganded binding protein to the membrane complex (equals k_{-2}/k_{+2} in Figure 1). Since it is assumed that both the liganded and the unliganded binding protein interact with the membrane complex, M (*18*−*21*), binding of E to M can be described by

$$K_d^E = \frac{E \cdot M}{E:M} \quad (10)$$

where K_d^E represents the binding constant of the unliganded binding protein to the membrane complex (equals k_{-4}/k_{+4} in Figure 1).

When two species are competing for the same binding site, as is the case for E and EL with M, the ratio of the bound species is given by

$$\frac{EL:M}{E:M} = \frac{K_d^E \cdot EL}{K_d^{EL} \cdot E} \quad (11)$$

which rearranges to

$$E:M = \frac{K_d^{EL} \cdot EL:M \cdot E}{K_d^E \cdot EL} \quad (12)$$

To obtain a relationship between M and L and E:M and L, EL has been eliminated from eqs 9 and 12, using eq 8, which yields

$$M = \frac{K_d^{EL} K_d^L \cdot EL:M}{E \cdot L} \quad (13)$$

$$E:M = \frac{K_d^{EL} K_d^L \cdot EL:M}{K_d^E \cdot L} \quad (14)$$

Because k_{+3} is relatively large, E:ML (Figure 1) will be a minor fraction of the total concentration of M, the molar fraction of EL:M can be given by

$$\frac{EL:M}{M_{tot}} = \frac{EL:M}{M + E:M + EL:M} \quad (15)$$

By combining eqs 10, 13, 14, and 15, one obtains a description of the molar fraction of EL:M as a function of L:

$$EL:M = \frac{M_{tot} \cdot L}{K_d^L \left(\frac{K_d^{EL}}{E} + \frac{K_d^{EL}}{K_d^E} \right) + L} \quad (16)$$

Because the term K_d^{EL}/E is likely to be small compared to the term K_d^{EL}/K_d^E, i.e., the concentration of the binding protein is assumed to be in the millimolar range (*2*), whereas both the K_d^E and K_d^{EL} are estimated to be in the micromolar range and more or less similar (*18*), the term K_d^{EL}/E can be neglected. Then, by combining eqs 7 and 16, one obtains the relation between v, K_d^L and L:

$$v = \frac{k'_{+2} M_{tot} L}{K_d^L \frac{K_d^{EL}}{K_d^E} + L} \quad (17)$$

Protein Determination. Protein concentrations of total cell lysates were determined with the Lowry protein assay using bovine serum albumin as standard. The concentration, purity, and stability of the purified OppA* were assessed by measuring the absorption spectrum of the sample between 240 and 340 nm on an Cary 100 spectrophotometer, assuming a calculated extinction coefficient of 1.605 (mg/mL)$^{-1}$ cm^{-1} or 102 700 M^{-1} cm^{-1} for OppA* (*22*).

RESULTS

*Expression and Purification of OppA**. Plasmid pAMP21 was introduced into *L. lactis* strain AMP2, which resulted in a 5−10-fold overproduction of OppA (Picon, A., Lanfermeijer, F. C., Kunji, E. R. S., Konings, W. N., and Poolman, B., unpublished results). Since OppA* lacks the class II signal peptide, the protein is not exported and does not contain the modification of the N-terminal cysteine that anchors the wild-type protein to the external face of the cell membrane. After breaking the cells and separating the cytoplasmic fraction from the debris and the membrane fraction, the cytoplasmic fraction was passed over an anion-exchange column (Source 30Q). Contrary to what was expected (the calculated pI of OppA* is 8.7), part of OppA* was retarded on the anion-exchange resin. The flow through, combined with the 200 mM KCl eluate (low salt fraction), and the 400 mM KCl eluate (high salt fraction) contained approximately 70 and 30% of OppA*, respectively (Figure 2). We speculate that this complex behavior of OppA* on the anion-exchange resin is due to interaction with other proteins or nucleic acids, present in the homogenate. In this regard, it is worth mentioning that "chaperone-like" activity has been reported for homologues of OppA (*23*, *24*). Although the anion-exchange step did not remove many contaminating proteins, it added tremendously in the further purification by removing nucleic acids.

The second step in the purification consisted of passage of the Source 30Q-fractions over a cation-exchange column (Resource S). Under the used conditions, this step was very efficient; only OppA* bound to the column, and more than 98% of the loaded protein eluted in the flow-through. Both the low- and high-salt fractions of the source 30 Q yielded OppA* that eluted from the resource S column at a salt concentration of about 270 mM. The elution profile around 270 mM KCl (Figure 3A) displayed heterogeneity, which manifested itself as a shoulder left or right of the main peak or in extreme cases as two peaks. Analysis of the individual fractions by SDS−PAGE (Figure 3B) and immunoblotting (data not shown) demonstrated that the two peaks correspond to OppA*. NCE, on the other hand, revealed the presence of at least two protein species in each of the peak fractions (Figure 3C). A slowly migrating species was dominant in the first fractions, whereas a faster migrating species was dominant in the later fractions. Incubation of the fractions with the peptide SLSQSKVLPVPQ transformed the slow-

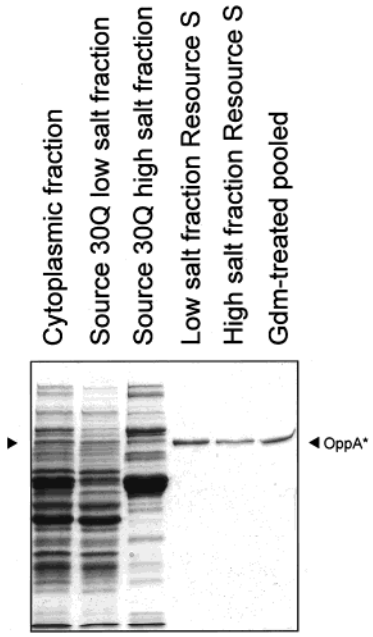

FIGURE 2: SDS−PAGE of the various fractions of the OppA*-purification. Lane 1, cytoplasmic fraction, 10 μg of protein was loaded; lane 2, source Q-fraction 0−200 mM KCl; lane 3, source Q-fraction 200−400 mM KCl; lane 4, OppA* purified from the 0−200 mM KCl-fraction; lane 5, OppA* purified from the 200−400 mM KCl-fraction; lane 6, Gdm-treated OppA*. One microgram of protein was loaded into lanes 4, 5, and 6.

migrating species into the fast-migrating one (Figure 3D). This strongly suggests that the two species observed by NCE are two conformations of OppA*: a liganded form (the fast-migrating species) and an unliganded form (the slow-migrating one). Finally, the overall procedure yielded approximately 2.5 mg of protein with a purity of >95% per liter of cell culture ($OD_{660} \approx 3$).

Removal of Endogenous Ligand. The presence of liganded OppA* was a major obstacle for further studies. Therefore, the ligand was removed by partially unfolding OppA* in guanidinium-HCl (Gdm). The unfolding and refolding resulted in OppA* protein completely devoid of endogenous ligand and fully active as judged by NCE (Figure 4). The Gdm-treated protein showed a red shift in the emission spectrum when compared with untreated purified OppA*. The increases in fluorescence at 315 nm, induced by the addition of saturating concentrations of the peptide SLSQSKVLP to both the untreated and Gdm-treated OppA*, were 3 and 12%, respectively (data not shown).

Assessment of Peptide Specificity by Native Cationic Electrophoresis. Incubation of OppA* with various ligands revealed that certain peptides were able to induce a mobility shift of the protein, whereas others were not (Figure 4A). Moreover, the capacity of peptides to induce the shift appeared to be concentration dependent. The peptides with an apparent high affinity were SLSQSKVLP, SLSQSKVLPVPQ, RDMPIQAF, and RDMPIQAFLLY; these peptides already induced a mobility shift at a concentration of 0.1 mM. Other peptides such as AA, AAA, AAAA, KGGK, KYGK, GLGL, and YGGFL were unable to induce a shift even at 1 mM. The peptides, AA and AAA, were not expected to cause a mobility shift as these peptides are not transported by Opp (*12*). The other peptides are most likely low-affinity ligands of OppA, because they are transported

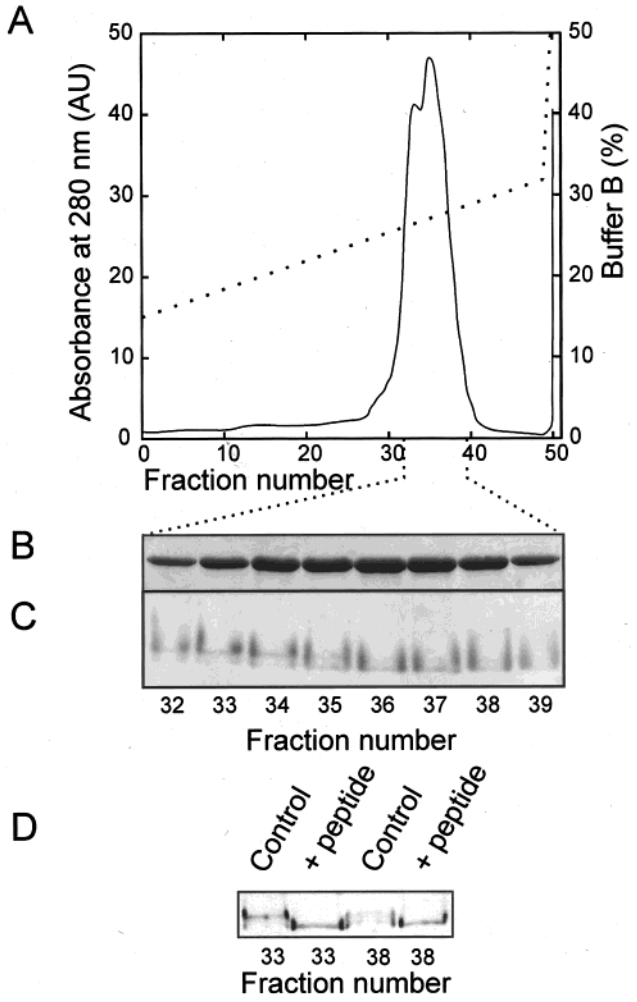

FIGURE 3: Analysis of the cation exchange fractions. (A) Elution profile of the cation exchange (Resource S) column. The solid line indicates the absorbance at 280 nm, The dotted line indicates the percentage of buffer B. (B) SDS−PAGE of the peak fractions. Eighteen microliters of sample was loaded; this corresponded to 1 μg of protein for fraction 37. (C) Native cationic electrophoresis of the peak fractions. One microgram of protein was loaded. (D) Native cationic electrophoresis of fractions 33 and 38. One microgram of protein was loaded. Protein samples were incubated for 5 min. at room temperature with and without 200 μM of the peptide SLSQSKVLPVPQ before loading.

by Opp (*12*), and, as is shown for SLSQS, a partial mobility shift was observed at concentrations of 10 and 25 mM (Figure 4B). Incubation of OppA* with bradykinin and pentaalanine (Figure 4A) resulted in a reproducible, but less pronounced, increase in mobility compared to the high-affinity peptides. This implies that binding of these peptides either provokes a different conformational state of the protein or that the extent of the mobility shift is affected by the type of peptide bound.

Peptide Binding Observed by Intrinsic Protein Fluorescence. OppA* has a fluorescence spectrum with an emission peak at 332 nm. Upon binding of high affinity peptides, a blue shift of approximately 2 nm combined with an increase in total fluorescence was observed (Figure 5). Binding of SLSQSKVLP (Figure 5A), RDMPIQA, and RDMPIQAF (data not shown) resulted in an increase in fluorescence between 290 and 350 nm, whereas the spectra were nearly superimposable above 350 nm. Binding of SLSQSKVLPVPQ (Figure 5B) and bradykinin (RPPGFSPFR; data not shown),

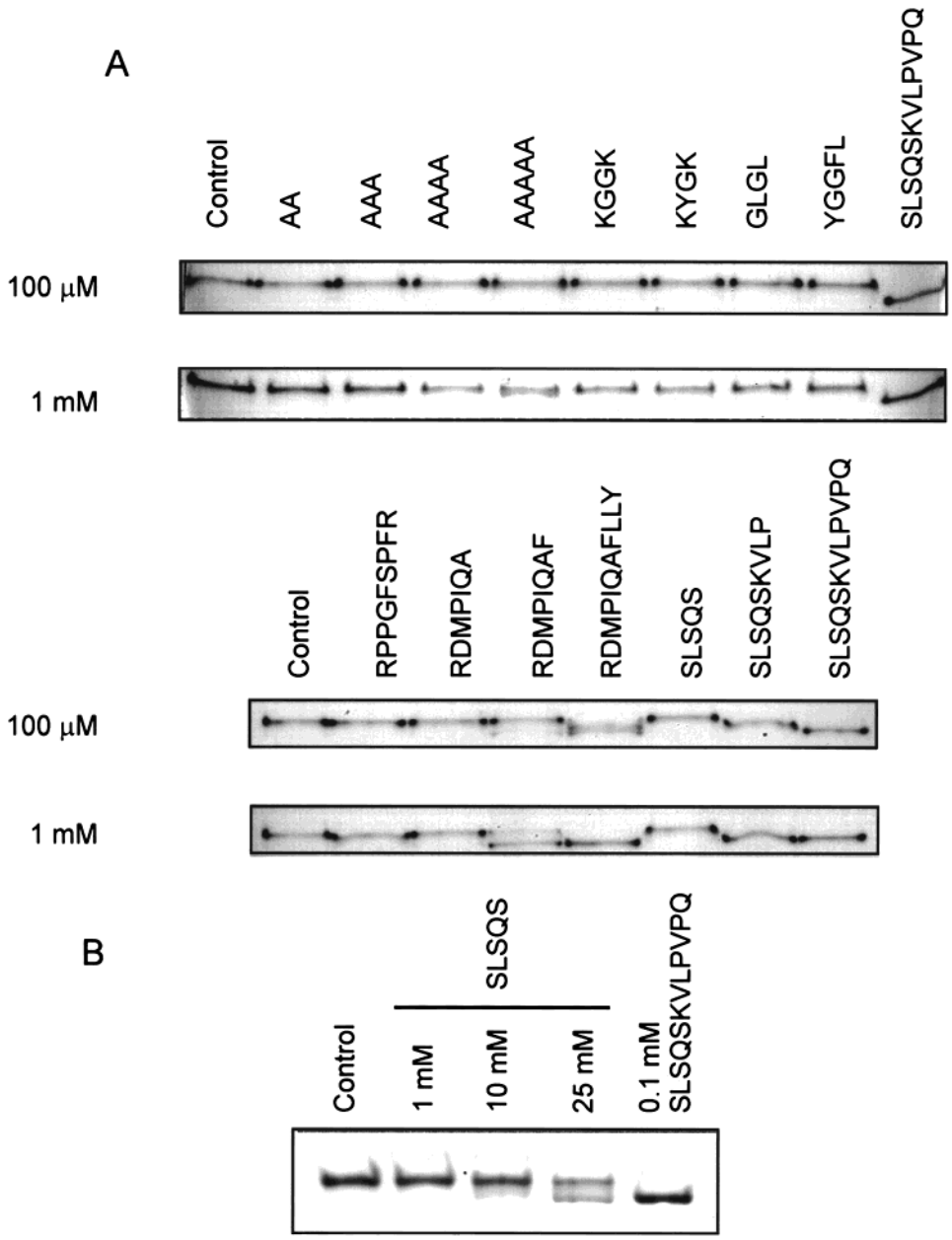

FIGURE 4: Peptide binding to OppA* as analyzed by native cationic electrophoresis. (A) Peptide specificity of OppA*. (B) SLSQS concentration dependence of the mobility shift of OppA* on native cationic electrophoresis gels. In both panels A and B, 1 μg of protein was loaded. Samples of purified and Gdm-treated OppA were incubated for 5 min. at room temperature with the indicated peptides at the indicated concentrations.

on the other hand, resulted in an increase in fluorescence below 340 nm and a reproducible decrease above 340 nm. The amplitude of the fluorescence change at 315 nm was concentration dependent for all peptides and could, consequently, be used to determine the kinetic parameters for peptide binding to OppA*. The β-casein-related peptides SLSQSKVLP, SLSQSKVLPVPQ, RDMPIQA, RDMPIQAF, and the noncasein-related peptide bradykinin bound to OppA* with simple saturable binding kinetics (Figure 6). The binding constants (K_d^L), however, varied widely, i.e., from 121 μM for RDMPIQA to 0.1 μM for bradykinin (Table 1). The binding of SLSQSKVLPVPQ was analyzed both by the fluorescence decrease at 340 nm and fluorescence increase at 315 nm. Both experiments yielded comparable K_d-values The high-affinity binding of bradykinin allowed us to determine the binding stoichiometry, which was 1.08 $\pm$ 0.08 peptide/protein molecule. This value justifies the usage of eq 2 for the analysis of the concentration dependence of bradykinin binding (Experimental Procedures).

The low-affinity peptide SLSQS also induced changes in the emission spectrum, but as expected, high concentrations of the peptide were needed. For instance, addition of 500 μM SLSQS induced a small, but reproducible, ~2% increase of the fluorescence at 315 nm. Moreover, 500 μM SLSQS increased the apparent K_d^L of OppA* for SLSQSKVLP from 2.0 to 2.9 μM and reduced the ΔF_{max} from 13.8 to 11.2%. These observations allowed us to approximate a K_d^L for SLSQS binding of 1−3 mM, assuming that SLSQS and SLSQSKVLP compete with each other for binding to OppA*.

Pre-Steady-State Kinetics of Peptide Binding to OppA. To determine whether the differences in the K_d^L-values for SLSQSKVLP, SLSQSKVLP, RDMPIQA, and RDMPIQAF

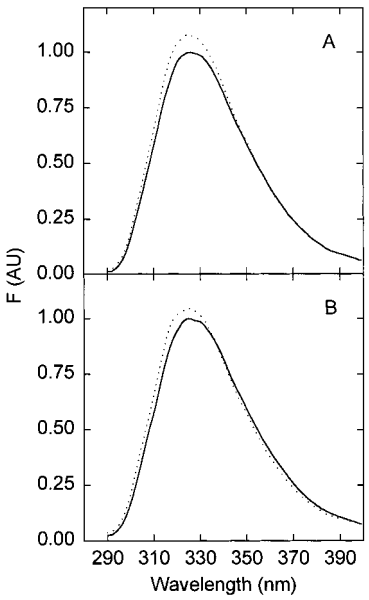

FIGURE 5: Effect of saturating concentrations of peptide on the intrinsic protein fluorescence of OppA*. Emission spectra were recorded in the absence (solid lines) and presence (broken lines) of 30 μM of SLSQSKVLP (A) and 10 μM of SLSQSKVLPVPQ (B).

are due to variations in the association (k_{+1}) or dissociation (k_{-1}) rate constants or both, we analyzed the time dependence of both the association and dissociation process. The change in fluorescence due to the association of both SLSQSKVLP and RDMPIQAF could be described by a single-exponential function. Data typical for the association of SLSQSKVLP to OppA* are shown in Figure 7A. The concentration dependence of the rate constants for these association processes (Figure 8) allowed us to assess the k_{+1}- and k_{-1}-values (Table 1). Association of the peptide RDMPIQA to OppA* was too rapid to be analyzed quantitatively. Even at low peptide concentrations (20 μM: $0.5 \times K_d^L$) the process was completed for at least 95% within 3 ms, which was just beyond the deadtime of 1.7 ms. This implies that the rate constant (k_{obs}) was > 920 s^{-1}. Consequently, we were only able to estimate the lower limits of the k_{+1}- and k_{-1}-rate constants, using the K_d^L-value obtained from the steady-state experiments (Table 1). Importantly, the ΔF_{eq}-values of the association process of RDMPIQA to OppA* displayed a concentration dependence similar to the data obtained in the steady-state experiments, which was also observed for the peptides SLSQSKVLP and RDMPIQAF.

The peptide SLSQSKVLPVPQ displayed different pre-steady-state binding kinetics. Its time dependence was biphasic; a rapid increase in fluorescence was followed by a slower decrease in the fluorescence signal (Figure 7B). These time curves were analyzed according a double exponential function. Both the observed rate constants of the first fast and second slow phase displayed concentration dependence and allowed us, assuming a two step association process involving isomerization of the liganded binding protein, to calculate the rate constants of the four partial reactions for SLSQSKVLPVPQ binding (*25*) (see legend to Table 1).

The dissociation process of SLSQSKVLP and RDMPIQAF could be described by a single-exponential decay curve with observed rate constants of 15 (final concentration = 0.83 μM) and 162 s^{-1} (final concentration = 16.7 μM), respectively (Figure 9; Table 2). These values agree well with predicted rate constants estimated from the k_{+1}- and k_{-1}-values obtained from the association reactions. The dissociation process of RDMPIQA could not be analyzed, because the process was too rapid. Dissociation of SLSQSKVLPVPQ from OppA* did not result in changes in fluorescence, which is consistent with the two step process and the values of the relevant rate constants.

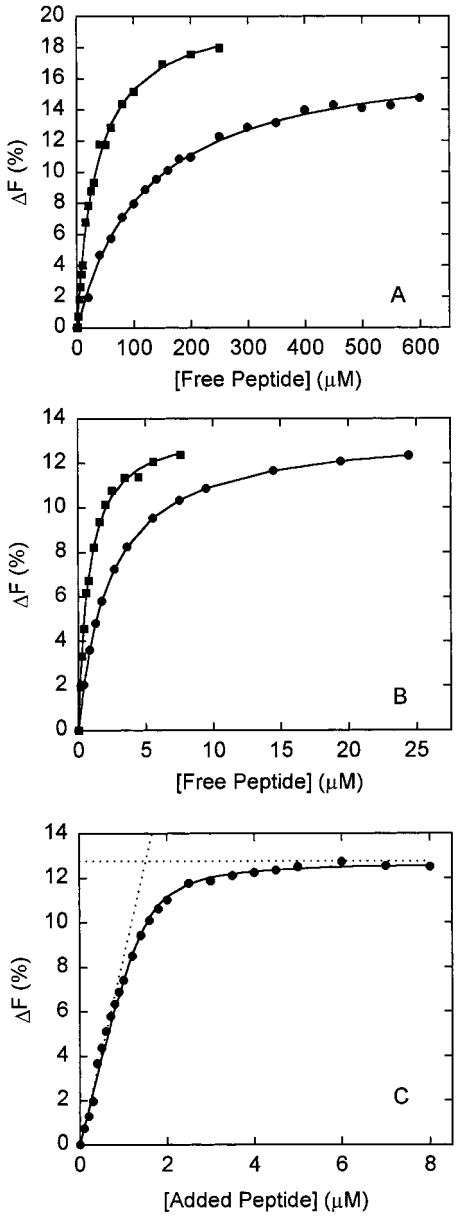

FIGURE 6: Concentration dependence of the fluorescence increase induced by various peptides. (A) RDMPIQA (●) and RDMPIQAF (■); (B) SLSQSKVLP (●) and SLSQSKVLPVPQ (■). (C) RPPGFSPFR. In panel C, the intercept of the two dotted lines is at a peptide concentration of 1.53 μM, the concentration of OppA* in this experiment was 1.49 μM. Data were analyzed according eqs 1 or 2 as described in the Experimental Procedures. The solid lines through the data points represent the best fits.

Comparison of the k_{+1}- and k_{-1}-rate constants for the different peptides showed that the k_{+1}-values varied at the most 2−3-fold, whereas the k_{-1}-values varied up to 2 orders of magnitude. Thus, the observed variations in the K_d^L-values are primarily the result of variation in the dissociation rate constants.

Table 1: Kinetic Parameters of Peptide Binding to OppA* and Inhibition Constants for Transport

peptide	number of residues	ΔF_{max} (%)	K_d^L (μM)	k_{+1} (μM^{-1} s^{-1})	k_{-1} (s^{-1})	k_{-1}/k_{+1} (μM)	K_i[a] (μM)
SLSQS	5	nd	>1000				82
SLSQSKVLP	9	13.4 ± 0.1	2.17 ± 0.07	7.3 ± 0.3	13.1 ± 4.2	1.8	23
SLSQSKVLPVPQ	12	13.7 ± 0.2	0.77 ± 0.03	6.6[b]	6.9[b]	1.1	17
RDMPIQA	7	18.0 ± 0.3	121.1 ± 0.5	~5.4[c]	~650[c]	30	
RDMPIQAF	8	20.0 ± 0.5	37.7 ± 2.4	2.8 ± 0.2	105.4± 11.5	37.7	33
RPPGFSPFR	9	12.6 ± 1.5	0.10 ± 0.02				nd

[a] From Detmers et al. (*12*); K_i, inhibition constant for peptide uptake. [b] Apparent rate constants $k_{+1}^{\#}$ and $k_{-1}^{\#}$ estimated according eqs A and B. Association curves obtained with the peptide SLSQSKVLPVPQ were analyzed assuming a two-step association process involving isomerization of the liganded binding protein (*25*):

$$E + L \underset{k_{-1}}{\overset{k_{+1}}{\rightleftharpoons}} EL_1 \underset{k_{-2}}{\overset{k_{+2}}{\rightleftharpoons}} EL_2$$

E, EL_1, and EL_2 are the unloaded and two isomers of the liganded binding protein, respectively. The following values for the rate constants were obtained: k_{+1}, 6.6 μM^{-1} s^{-1}; k_{-1}, 74.6 s^{-1}; k_{+2}, 46.6 s^{-1} and k_{-2}, 4.8 s^{-1}. The apparent $k_{+1}^{\#}$ and $k_{-1}^{\#}$ rate constants could be derived from k_{+1}, k_{-1}, k_{+2}, and k_{-2}, when one assumes the total amount of liganded binding protein (EL_t) to be the sum of EL_1 and EL_2:

$$E + L \underset{k_{-1}^{\#}}{\overset{k_{+1}^{\#}}{\rightleftharpoons}} EL_t$$

Using this assumption, the following relations are obtained and these were used to calculate the apparent rate-constants:

$$k_{+1}^{\#} = k_{+1} \qquad \text{(A)}$$

$$k_{-1}^{\#} = \frac{k_{-1}k_{-2}}{k_2 + k_{-2}} \qquad \text{(B)}$$

[c] Estimated from the observation that the association process is completed within 3 ms, which results in a rate constant, k, of >920 s^{-1}. The k_{+1} and k_{-1} are calculated using K_d^L and eq 4.

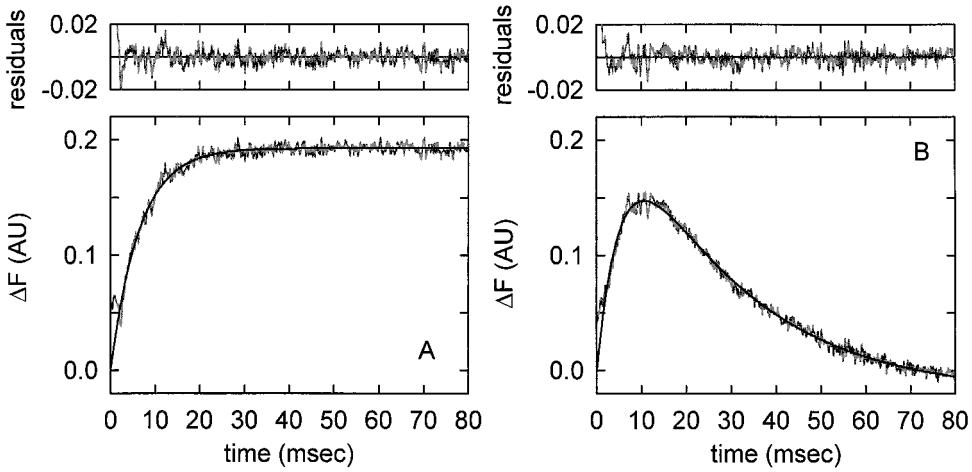

FIGURE 7: Typical pre-steady-state fluorescence changes for peptide association to OppA*. (A) SLSQSKVLP (20 μM); (B) SLSQSKVLPVPQ (20 μM). Grey lines are the experimentally obtained data sets. Data were analyzed according eqs 3 and 5 for SLSQSKVLP and SLSQSKVLPVPQ, respectively. The black lines through the data points represent the best fits. Residuals are given in the small panels above the main figures.

DISCUSSION

In this paper, we present solid kinetic data on the binding of peptides, varying in length from 5 to 12 amino acid residues, to the oligopeptide-binding protein (OppA*) of *L. lactis*. OppA* corresponds to the oligopeptide binding protein of *L. lactis* without the N-terminal lipid modification; OppA* was produced intracellularly because of the deletion of its export signal. Binding of peptides to OppA* results in conformational changes in the protein that are observed by both native cationic electrophoresis and intrinsic protein fluorescence. Analysis of the pre-steady-state and steady-state peptide binding kinetics by intrinsic protein fluorescence showed that (1) the affinity of OppA* for peptides increases with increasing length of the ligand, (2) the affinity varies from 0.1 μM (RPPGFSPFR) to >1 mM (SLSQS), and (3) the variations in affinities result primarily from differences in dissociation rate constants. The binding of such long peptides to OppA* is discussed in relation to the known binding mechanism that was postulated on the basis of different structures of the homologous oligopeptide binding protein of *S. typhimurium* ($OppA_{st}$). $OppA_{st}$ is thought to bind peptides with at most five amino acid residues as the size of its binding site does not give indications about the accommodation of longer peptides. The implications of the binding kinetics for the transport of peptides via the Opp-system are also discussed.

*Structural Implications of the Binding of Long Peptides by OppA**. The three-dimensional structures of the peptide binding proteins of the Dpp-system of *E. coli* ($DppA_{Ec}$) and Opp-system of *S. typhimurium* ($OppA_{St}$) have been determined with and without their respective ligands (*4*, *5*, *8*−*11*). In both proteins, salt bridges are formed between the amino-

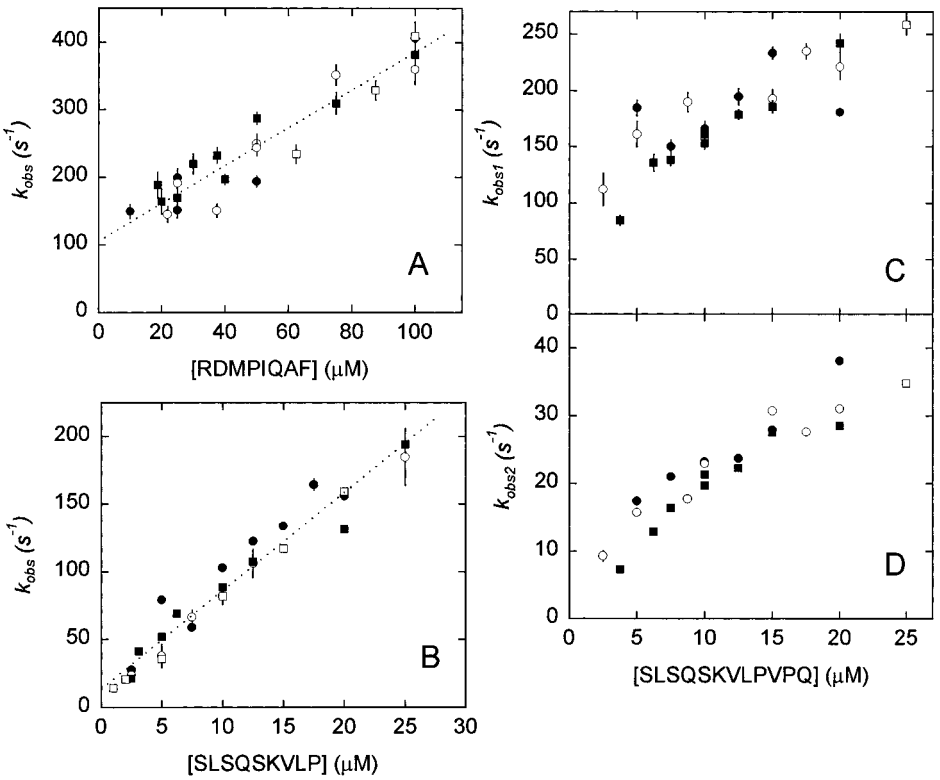

FIGURE 8: Concentration dependence of the observed rate constants of the pre-steady-state association process for the various peptides. (A) RDMPIQAF, the dotted line represents the best line through the data set; (B) SLSQSKVLP, the dotted line represents the best line through the data set; (C) SLSQSKVLPVPQ. The various symbols represent different experiments and the bars indicate standard errors, resulting from the kinetic analysis. In the case of RDMPIQAF and SLSQSKVLP, the values for k_{+1} and k_{-1} were obtained from the slope and the intercept of the line with the *y*-axis, respectively (Table 1).

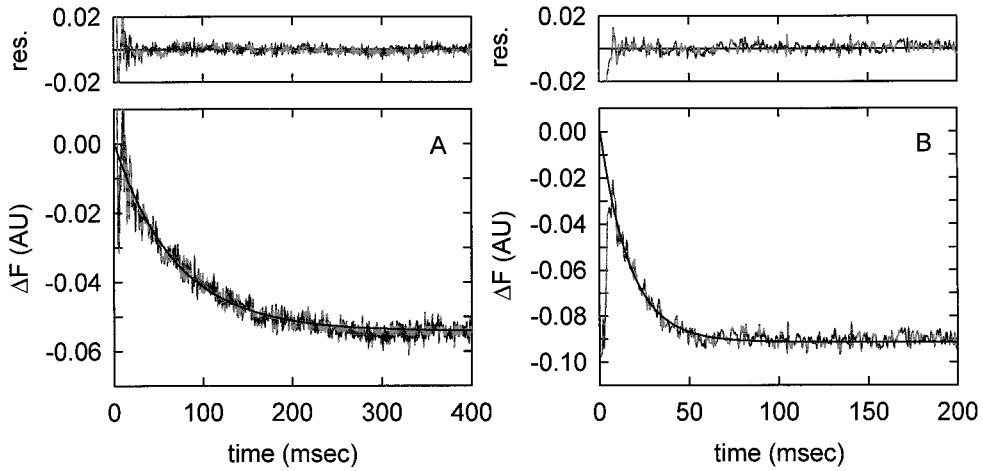

FIGURE 9: Typical pre-steady-state fluorescence changes for peptide dissociation from OppA*. (A) SLSQSKVLP (final concentration, 0.83 μM); (B) RDMPIQAF (final concentration, 16.7 μM). Grey lines are the experimentally obtained data sets. Data were analyzed according eqs 6. The black lined through the data sets represent the best fits. Residuals are given in the small panels above the main figures.

and carboxyl-terminus of the peptide and oppositely charged residues in the binding protein. A large number of hydrogen bonds is formed between the peptide backbone and the protein; these interactions can be described as parallel and antiparallel β-sheet (*5*). The side chains of the peptide residues are accommodated in hydrated pockets (*10*). A variable number of water molecules allow the pockets to accommodate side chains of variable size. Also, the water molecules participate in hydrogen bonding between the side chains and protein residues, and they are able to dissipate charges of the ligand. Apolar side chains can be accommodated because the hydrophilic moieties in the pocket can form hydrogen bonds with each other with and without the participation of the water molecules (*5*). Since OppA of *L. lactis* ($OppA_{Ll}$) is homologous to $DppA_{Ec}$ and $OppA_{St}$, the $OppA_{Ll}$ protein is likely to have a comparable mode of binding. It should be stressed, however, that $OppA_{Ll}$ is most distantly related to these proteins within the family, and that critical residues, involved in peptide binding in $OppA_{St}$, are not easily recognized in the primary sequence of $OppA_{Ll}$ (Picon, A., Lanfermeijer, F. C., Kunji, E. R. S., Konings, W. N., and Poolman, B., unpublished results).

The crystal-structure of $OppA_{St}$ has revealed how di-, tri-, and tetrapeptides are accommodated in the binding site. Also, it provides a clue toward the binding of pentapeptides. It appears that a pentapeptide is totally occluded from the

Table 2: Observed and Estimated Rate Constants for the Dissociation Processes as Presented in Figure 9

peptide	number of residues	final concentration (μM)	k_{obs}[a] (s^{-1})	k_{est}[b] (s^{-1})
SLSQSKVLP	9	0.83	15.4 ± 2.9	19.2 ± 4.5
RDMPIQAF	8	16.7	162.5 ± 14.7	152.1 ± 14.8

[a] The observed dissociation rate constant, k_{obs}, was obtained by analyzing the dissociation processes according eq 6. [b] The estimated rate constant, k_{est}, was obtained from the data in Table 1 and using eq 4.

medium when the protein is in the closed liganded state. It is unlikely, however, that peptides with more than five residues, if bound, will be totally occluded. One would predict that these peptides will partially stick out of the protein.

The Opp-system of *L. lactis* mediates the transport of peptides ranging in size from 4 to 18 amino acid residues (*12*) and the binding of typical peptides of 5−12 residues is characterized in this paper. Although the number of peptides used is limited, our data clearly indicate that residues in excess of five highly contribute to the affinity of OppA* for peptides. When we assume that the binding domains of $OppA_{St}$ and $OppA_{Ll}$ are similar, one must conclude that the additional amino acids of the peptides longer than five residues interact with the surface of the protein. Indeed, preliminary experiments, using nonameric peptides with a cysteine for labeling with fluorophores at either position 1, 3, 4, 5, 6, 7, or 9, indicate that the first five residues are occluded in the binding protein, whereas the remaining four are surface exposed. The interaction of the exposed peptide residues with the surface of OppA must be rather strong as the K_d^L of SLSQSKVLP is nearly 3 orders of a magnitude smaller than that of SLSQS. Although the transport or binding of "long" oligopeptides by Opp systems other than $OppA_{Ll}$ has not been studied thoroughly, it is possible that these systems have a similar capacity.

Two Different Responses Can Be Observed upon Peptide Binding. In general, it is assumed that binding of ligands to binding proteins involves a two-step process: binding of the ligand to the open form of the binding protein, which is followed by closure of the binding protein (*6*, *7*). Since the nona-, deca-, and dodecapeptides all provoked a conformational change in OppA*, as shown by the native cationic electrophoresis experiment, it is most plausible that closure of the binding protein is occurring. Therefore, the single exponential rise curve, observed with the peptides RDMPIQAF and SLSQSKVLP, reflects both binding to and closure of the binding protein. This implies that the steps of binding and closure of the binding protein are kinetically inseparable and suggests that closure of the binding protein is much faster than the initial binding step. This type of kinetics has also been observed for ligand binding to other binding proteins (*17*). Although the pre-steady-state analysis of binding of SLSQSKVLPVPQ reveals two kinetic components, it is unlikely that the principle binding mechanism is different from that of SLSQSKVLP and RDMPIQAF. We suggest that the complex pre-steady-state kinetics of SLSQSKVLPVPQ shows the interaction of the N-terminal residues of the peptide with the binding pocket (increase in fluorescence) as well as additional interaction of the C-terminal residues with the surface residues of the binding protein (subsequent decrease in fluorescence). The additional interaction between OppA* and the ligands also occurs with the nona- and undecameric peptides, but they are not reported by the fluorescence assay (different local environments).

Relation between Binding and Transport Affinities. The various peptides used in this study were previously found to be taken up by Opp of *L. lactis* with non-Michealis-Menten kinetics, which contrasts with the saturable kinetics of peptide binding reported here. Moreover, the variations in affinity constants for transport (K_m or K_i) are much smaller than the variations in K_d^L-values (Table 1). Thus, the same peptides that display more than a 1000-fold difference in K_d^L display only 10-fold difference in K_m or K_i for transport. Depending on the type of peptide, the K_d^L can be larger or smaller than the K_m. This is quite unusual as the K_m- and K_d^L-values agree rather well for most binding protein dependent transport systems. In other words, the K_m-values for the transport systems usually reflect the K_d^L-values for substrate binding (*2*).

Three possible explanations for the observed differences in uptake and binding affinities can be formulated. First, the differences could partly be methodological as we cannot exclude that in the in vivo transport assays the peptide concentration, experienced by the binding protein, differs from the concentration in the solution due to interference of peptides with the cell wall. Second, the oligomerization state of the protein could differ in vivo and in vitro as the effective concentration of OppA, anchored to the cell membrane will be much higher than the concentrations used in our binding experiments. If oligomerization occurs, it will be most prominent at high protein concentrations and cooperatively in ligand binding may be observed. (*26*). Third, depending on which step(s) is rate determining in the translocation process, the K_m for transport may or may not reflect the K_d^L of binding.

The kinetic data are analyzed in the light of the kinetic model (Scheme 1). Where E and EL represent the unloaded and liganded binding protein, respectively, L_o and L_i are the external and internalized substrate, respectively, and M refers to the membrane complex. The species EL:M and E:M represent loaded and unloaded binding proteins docked to membrane complex, respectively. E:ML refers to the situation in which the ligand is transferred to the membrane complex and the binding protein is still docked. The following steps are discriminated in the model: I, binding of ligand to the binding protein; II, docking of the liganded binding protein to the membrane complex; III, donation of the ligand to the membrane complex; IV, translocation of substrate across the membrane (Figure 1). The branch with the constants k'_{+1} and k'_{-1} provides an explanation for the sigmoidial uptake kinetics (see ref *12*). If step III, governed by the constant k'_{+2}, is rate determining, then the rate of transport can be described by

$$v = \frac{k'_{+2} \cdot M_{tot} \cdot L}{K_d^L \frac{K_d^{EL}}{K_d^E} + L} \qquad (17)$$

This equation (see under Experimental Procedures) has the form of a simple Michaelis−Menten relationship, in which the K_m for transport equals K_d^L (K_d^{EL}/K_d^E). Thus, when

one assumes that the ratio K_d^{EL}/K_d^E is independent of the type of peptide bound, then K_m-values are expected to vary along with the K_d^L-values for binding of the peptides to the binding protein. Miller et al. (*17*) tested the assumption that k'_{+2} is rate determining for several binding protein-dependent systems and reached the conclusion that it was not. However, they considered the total concentration of liganded binding protein instead of the concentration of liganded binding protein that is associated with the membrane components. Because the concentration of membrane components can be 1−2 magnitudes lower than the concentration of binding protein (*2*, *27*) the concentration of docked liganded binding protein, and therefore, the potential donation rates will be overestimated.

In case k'_{+2} does not significantly determine the rate of transport, then the preceding steps will not reach equilibrium and the K_m for transport will become smaller than the K_d^L. Thus, the difference in the variation in K_m- and K_d^L-values for different peptides can to a large extent be explained when one assumes that the dissociation rate constant (k'_{+2}) varies largely for the different peptides.

Our pre-steady-state kinetic experiments showed that the k_{+1}-values for all peptides studied varied at most 2−3-fold, whereas the k_{-1}-values could vary at least 100-fold (Table 1). Thus, the variations observed for the K_d^L-values were mainly due to variations in k_{-1}-values. When we assume that k'_{+2} and k_{-1} (Figure 1) are related, or in other words, the rate of dissociation of the peptide from the binding protein is the same for "free" and "membrane-docked" binding protein, then "low-affinity" peptides are donated more rapidly to the membrane complex than high-affinity peptides. This implies that, for the peptides that bind with a high affinity, the donation rate constant (k'_{+2}) could be rate determining, and therefore, the K_m will reflect the K_d^L, whereas in case of the peptides that bind with a low affinity, a high transport affinity may be obtained because step III is no longer rate determining.

ACKNOWLEDGMENT

We acknowledge the technical and theoretical support of Dr. J. Broos of the Biochemistry Department of the University of Groningen during the stopped-flow experiments.

REFERENCES

1. Higgins, C. F. (1992) *Annu. Rev. Cell Biol. 8*, 67−113.
2. Ames, G. F. (1986) A*nnu. Rev. Biochem. 55*, 397−425.
3. Tam, R., and Saier, M. H. (1993) *Microbiol. Rev. 57*, 320−346.
4. Nickitenko, A. V., Trakhanov, S., and Quiocho, F. A. (1995) *Biochemistry 34*, 16585−16595.
5. Tame, J. R., Murshudov, G. N., Dodson, E. J., Neil, T. K., Dodson, G. G., Higgins, C. F., and Wilkinson, A. J. (1994) *Science 264*, 1578−1581.
6. Mao, B., Pear, M. R., McCammon, J. A., and Quiocho, F. A. (1982) *J. Biol. Chem. 257*, 1131−1133.
7. Sack, J. S., Saper, M. A., and Quiocho, F. A. (1989) *J. Mol. Biol. 206*, 171−191.
8. Dunten, P., and Mowbray, S. L. (1995) *Protein Sci. 4*, 2327−2334.
9. Tame, J. R., Dodson, E. J., Murshudov, G., Higgins, C. F., and Wilkinson, A. J. (1995) *Structure 3*, 1395−1406.
10. Tame, J. R., Sleigh, S. H., Wilkinson, A. J., and Ladbury, J. E. (1996) *Nat. Struct. Biol. 3*, 998−1001.
11. Sleigh, S. H., Tame, J. R. H., Dodson, E. J., and Wilkinson, A. J. (1997) *Biochemistry 36*, 9747−9758.
12. Detmers, F. J. M., Kunji, E. R. S., Lanfermeijer, F. C., Poolman, B., and Konings, W. N. (1998) *Biochemistry 37*, 16671−16679.
13. Kunji, E. R., Fang, G., Jeronimus-Stratingh, C. M., Bruins, A. P., Poolman, B., and Konings, W. N. (1998) *Mol. Microbiol. 27*, 1107−1118.
14. Kunji, E. R., Mierau, I., Poolman, B., Konings, W. N., Venema, G., and Kok, J. (1996) *Mol. Microbiol. 21*, 123−131.
15. Laemmli, U. K. (1970) *Nature 227*, 680−685
16. Reisfield, R. A., Lewis, U. J., and Williams, D. E. (1962) *Nature 195*, 281−283.
17. Miller, D. M., Olson, J. S., Pflugrath, J. W., and Quiocho, F. A. (1983) *J. Biol. Chem. 258*, 13665−13672.
18. Ames, G. F. L., Liu, C. E., Joshi, A. K., and Nikaido, K. (1996) *J. Biol. Chem. 271*, 14264−14270.
19. Bohl, E., and Boos, W. (1997) *J. Theor. Biol. 186*, 65−74.
20. Bohl, E., Shuman, H. A., and Boos, W. (1995) *J. Theor. Biol. 172*, 83−94.
21. Krupka, R. M. (1992) *Biochim. Biophys. Acta 1110*, 11−19.
22. Pace, C. N., Vajdos, F., Fee, L., Grimsley, G., and Gray, T. (1995) *Protein Sci. 4*, 2411−2423.
23. Matsuzaki, M., Kiso, Y., Yamamoto, I., and Satoh, T. (1998) *J. Bacteriol. 180*, 2718−2722.
24. Richarme, G., and Caldas, T. D. (1997) *J. Biol. Chem. 272*, 15607−15612.
25. Dixon, M., and Webb, E. C. (1979) *Enzymes*, pp 202−204, Longman Group Limited, London, U.K.
26. Richarme, G. (1982) *Biochem. Biophys. Res. Commun. 105*, 476−481.
27. Manson, M. D., Boos, W., Bassford, P. J., and Rasmussen, B. A. (1985) *J. Biol. Chem. 260*, 9727−9733.

BI9914715